

Experimental assessment of scale effects affecting two-phase flow properties in hydraulic jumps

Frédéric Murzyn · Hubert Chanson

Received: 14 December 2007 / Revised: 10 March 2008 / Accepted: 17 March 2008 / Published online: 7 April 2008
© Springer-Verlag 2008

Abstract A hydraulic jump is the rapid transition from a supercritical to subcritical free-surface flow. It is characterised by strong turbulence and air bubble entrainment. New air–water flow properties were measured in hydraulic jumps with partially developed inflow conditions. The data set together with the earlier data of Chanson (Air bubble entrainment in hydraulic jumps. Similitude and scale effects, 119 p, 2006) yielded similar experiments conducted with identical inflow Froude numbers $Fr_1 = 5$ and 8.5, but Reynolds numbers between 24,000 and 98,000. The comparative results showed some drastic scale effects in the smaller hydraulic jumps in terms of void fraction, bubble count rate and bubble chord time distributions. The present comparative analysis demonstrated quantitatively that dynamic similarity of two-phase flows in hydraulic jumps cannot be achieved with a Froude similitude. In experimental facilities with Reynolds numbers up to 10^5 , some viscous scale effects were observed in terms of the rate of entrained air and air–water interfacial area.

List of symbols

C void fraction defined as the volume of air per unit volume of air
 C_{\max} maximum void fraction in the air bubble diffusion layer

F. Murzyn
ESTACA Campus Ouest, Parc Universitaire de Laval - Changé,
Rue Georges Charpak, BP 76121, 53061 Laval Cedex 9, France

H. Chanson (✉)
Division of Civil Engineering, The University of Queensland,
Brisbane, QLD 4072, Australia
e-mail: h.chanson@uq.edu.au

D_t turbulent diffusivity (m^2/s) of air bubbles in air–water flow
 D^* dimensionless turbulent diffusivity: $D^* = \frac{D_t}{v_1 d_1}$
 d_{ab} bubble size (m)
 d_1 upstream flow depth (m)
 F bubble count rate (Hz), or bubble frequency (number of detected air bubbles per unit time)
 F_{\max} maximum bubble count rate (Hz) at a given cross-section
 Fr_1 upstream Froude number: $Fr_1 = V_1 / \sqrt{g d_1}$
 g gravity constant: $g = 9.80 \text{ m/s}^2$ in Brisbane, Australia
 L_{scale} geometric scaling ratio defined as the ratio of prototype to model dimensions
 Mo Morton number defined as: $Mo = g \mu^4 / (\rho \sigma^3)$
 N_{ab} number of air bubbles per record
 Q water discharge (m^3/s)
 q water discharge per unit width (m^2/s)
 Re Reynolds number: $Re = \rho V_1 d_1 / \mu$
 u' root mean square of longitudinal component of turbulent velocity (m/s)
 V interfacial velocity (m/s)
 W channel width (m)
 We Weber number
 x longitudinal distance from the upstream gate (m)
 x_1 longitudinal distance from the gate to the jump toe (m)
 y distance (m) measured normal to the channel bed
 $Y_{C_{\max}}$ distance (m) normal to the jet support where $C = C_{\max}$
 z transverse distance (m) from the channel centreline

Greek symbols

δ boundary layer thickness (m)
 μ dynamic viscosity of water (Pa s)

- ρ density (kg/m^3) of water
 σ surface tension between air and water (N/m)
 \varnothing diameter (m)

Subscript

- 1 upstream flow conditions

1 Introduction

The hydraulic jump is the rapid transition from a supercritical to a subcritical open channel flow. It is characterised by the interaction of a strong turbulence with a free surface leading to air entrainment with macro-scale vortices and kinetic energy dissipation (Fig. 1). A hydraulic jump is defined by its inflow Froude number $Fr_1 = V_1/\sqrt{gd_1}$ where V_1 is the inflow velocity, d_1 is the inflow depth and g is the gravity acceleration. Fr_1 is always greater than unity. Air bubble entrainment in a hydraulic jump starts for $Fr_1 > 1-1.3$ (Chanson 1997; Murzyn et al. 2007). The air entrainment is caused by the strong interaction between turbulence and free surface, which generates disturbances of the air–water interface and vortex formation leading to some air entrapment. Void fraction measurements in hydraulic jumps were first conducted by Rajaratnam (1962). Resch and Leutheusser (1972) performed hot-film probe measurements in the bubbly flow region and showed some effects of the upstream flow conditions. Recent developments included Chanson (1995), Mossa and Tolve (1998), Chanson and Brattberg (2000), Murzyn et al. (2005) and Chanson (2007a).

In this study, detailed air–water flow measurements were performed in hydraulic jump flows for two inflow

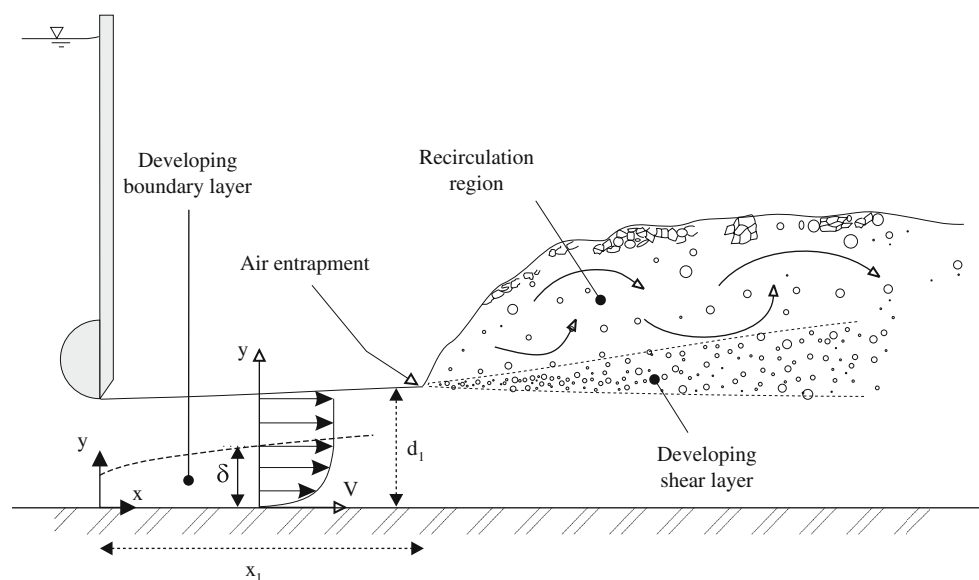
Froude numbers ($Fr_1 = 5, 8.5, Re = 38,000, 62,000$). The results were compared with an earlier study (Chanson 2006) performed with identical inflow Froude numbers but different geometric scales. The comparative analysis provides an assessment of scale effects affecting void fraction and bubble count rate distributions in hydraulic jumps with partially developed inflow conditions.

1.1 Dimensional analysis and similitude

Theoretical and numerical studies of air bubble entrainment in hydraulic jumps are difficult because of the large number of relevant equations (Chanson 1997; Chanson and Gualtieri 2008). Experimental investigations are performed with geometrically similar models based upon a dimensional analysis and dynamic similitude. In the study of the hydraulic jump, the Froude similitude is commonly used because of theoretical considerations (Bélanger 1828; Henderson 1966). But the turbulent processes in the shear region are dominated by viscous forces (Wood 1991; Chanson 1997).

For a hydraulic jump in smooth, horizontal, rectangular channels, a simplified dimensional analysis showed that the parameters affecting the air–water flow properties at a position (x, y, z) include: (a) the fluid properties including the air and water densities ρ_{air} and ρ , the air and water dynamic viscosities μ_{air} and μ , the surface tension σ , and the gravity acceleration g , (b) the channel properties including the width W , and, (c) the inflow properties such as the inflow depth d_1 , the inflow velocity V_1 , a characteristic turbulent velocity u'_1 , and the boundary layer thickness δ (Chanson 2006, 2007b). In addition, biochemical properties of the water solution must be considered and may have some

Fig. 1 Air entrainment in a hydraulic jump with partially developed inflow



significant effect. If the local void fraction C is known, the density and viscosity of the air–water mixture may be expressed in terms of the water properties and void fraction only; hence the parameters ρ_{air} and μ_{air} may be ignored. The result may be expressed in dimensionless terms:

$$C, \frac{Fd_1}{V_1}, \frac{V}{\sqrt{gd_1}}, \frac{u'}{V_1}, \frac{d_{\text{ab}}}{d_1} \dots = F_1 \left(\frac{x}{d_1}, \frac{y}{d_1}, \frac{z}{d_1}, Fr_1, \frac{u'_1}{V_1}, Re, Mo, \frac{x_1}{d_1}, \frac{\delta}{d_1}, \frac{W}{d_1}, \dots \right) \tag{1}$$

where F is the bubble count rate, V is the velocity, u' is a characteristic turbulent velocity, d_{ab} is a bubble size, x is the coordinate in the flow direction measured from the upstream gate, y is the vertical coordinate, z is the transverse coordinate measured from the channel centreline, and x_1 is the distance from the upstream gate (Fig. 1).

In Eq. (1), the dimensionless air–water flow properties at a dimensionless position $(x/d_1, y/d_1, z/d_1)$ within the jump are expressed as functions of the dimensionless inflow properties and channel geometry. In the right hand side of Eq. (1), the fourth, sixth and seventh terms are the inflow Froude number Fr_1 , Reynolds number $Re = \rho V_1 d_1 / \mu$ and Morton number $Mo = g \mu^4 / \rho \sigma^3$, respectively. Note that the Weber We was replaced by the Morton number since $Mo = We^3 / (Fr^2 Re^4)$. The Morton number is a function only of fluid properties and gravity constant, and it becomes an invariant if the same fluids (air and water) are used in both model and prototype, as in the present study.

The first systematic study of dynamic similarity and scale effects affecting the two-phase flow properties in hydraulic jumps was the work of Chanson (2006, 2007b). For two inflow Froude numbers ($Fr_1 = 5.1, 8.5$), the experiments tested the validity of the Froude similitude and the effects of the inflow Reynolds number, with all other relevant parameters being constant:

$$C, \frac{Fd_1}{V_1}, \frac{V}{\sqrt{gd_1}}, \frac{u'}{V_1}, \frac{d_{\text{ab}}}{d_1} \dots = F_2(Re) \tag{2}$$

where the Froude number Fr_1 and the relative channel width W/d_1 were constant: i.e. $Fr_1 = 5.1, 8.5, W/d_1 = 20$ (Table 1). The results of the Froude-similar experiments showed some scale effect in the smaller hydraulic jumps. In the same study, Chanson (2006) tested the effect of the relative width W/d_1 , with all other relevant parameters being constant. That is:

$$C, \frac{Fd_1}{V_1}, \frac{V}{\sqrt{gd_1}}, \frac{u'}{V_1}, \frac{d_{\text{ab}}}{d_1} \dots = F_3 \left(\frac{W}{d_1} \right) \tag{3}$$

where the inflow Froude and Reynolds numbers were constant: $Fr_1 = 5, 8.5, Re = 75,000, 95,000$ (Table 1). The results showed that the relative channel width had no effect on the air–water flow properties for:

$$\frac{W}{d_1} \geq 10 \quad \text{no effect of channel width} \tag{4}$$

In the present study, two experiments were conducted with the same inflow Froude numbers as the study of Chanson (2006) (Table 1). The instrumentation was similar for the present and earlier investigations, including identical sampling rate (20 kHz) and duration (45 s). A systematic comparison between the present and earlier data provides new information on the validity of the Froude similarity to study the two-phase flow properties in hydraulic jumps, particularly with reference to viscous scale effects. Note that the present study was conducted with a relative channel width $W/d_1 = 28$ which satisfied Eq. (4).

2 Experimental apparatus and procedures

New experiments were performed in a horizontal rectangular flume at the Gordon McKay Hydraulics Laboratory

Table 1 Summary of experimental flow conditions for detailed two-phase flow measurements in hydraulic jumps

Reference	x_1 (m)	d_1 (m)	Fr_1	Re	W (m)	Instrumentation	Sensor size (mm)	Sampling rate (Hz)	Sampling time (s)
Chanson (2006)	1.0	0.024	5.1	68,000	0.50	Single-tip conductivity	0.35	20,000	45
			8.6	98,000					
Present study	0.75	0.018	5.1	38,000	0.50	Dual-tip conductivity	0.25	20,000	45
			8.3	62,000					
Chanson (2006)	0.5	0.012	5.1	25,000	0.25	Single-tip conductivity	0.35	20,000	45
			8.4	38,000					
Chanson (2006)	1.0	0.024	5.0	77,000	0.25	Single-tip conductivity	0.35	20,000	45
			8.0	95,000					

Note: Hydraulic jumps with partially developed inflow conditions

of University of Queensland (Fig. 2). The channel width was 0.50 m. The sidewall height and flume length were respectively 0.45 and 3.2 m. The sidewalls were made of glass and the channel bed was PVC. This channel was previously used by Chanson (2006, 2007a).

The water discharge was measured with a Venturi meter located in the supply line and which was calibrated on-site with a large V-notch weir. The discharge measurement was accurate within $\pm 2\%$. The clear-water flow depths were measured using rail mounted point gages with a 0.2 mm accuracy. The inflow conditions were controlled by a vertical gate with a semi-circular rounded shape ($\varnothing = 0.3$ m) (Fig. 1). The upstream gate aperture was fixed during all experiments ($d_1 = 0.018$ m).

The air–water flow properties were measured with a double-tip conductivity probe (Fig. 2). The probe was equipped with two identical sensors with an inner diameter of 0.25 mm. The probe was manufactured at the University of Queensland and was previously used in several studies, including Chanson and Carosi (2007a). The conductivity probe is a phase-detection intrusive probe designed to pierce the bubbles. Its principle is based on the difference

in electrical resistance between air and water (Crowe et al. 1998; Chanson 2002). The dual-tip probe was excited by an electronic system (Ref. UQ82.518) designed with a response time of less than 10 μs . During the experiments, each probe sensor was sampled at 20 kHz for 45 s. The sampling rate and duration were selected based upon the outcomes of sensitivity analysis performed with phase-detection conductivity probes (Chanson 2006, 2007b). Depending upon the Froude number, three to four vertical profiles were recorded at different cross-sections downstream of the jump toe. Each vertical profile contained at least 30 points. The displacement and the position of the probe in the vertical direction were controlled by a fine adjustment system connected to a MitutoyoTM digimatic scale unit with a vertical accuracy Δy of less than 0.1 mm.

The analysis of the probe voltage output was based upon a single threshold technique, with a threshold set between 45 and 55% of the air–water voltage range. Below this threshold, the probe was in air whereas it was in water for larger voltage output voltages. The single-threshold technique is a robust method that is well suited to free-surface flows (Toombes 2002; Chanson and Carosi 2007b). The error on the void fraction was expected to be 1% using this technique.

For each experiment, the foot of the jump, or jump toe, was fixed at $x_1 = 0.75$ m and the upstream flow depth was $d_1 = 0.018$ m. Based on previous experiments made with the same experimental facility, the inflow was characterised by a partially-developed boundary layer. Further details on the experimental setup and results were reported in Murzyn and Chanson (2007).

3 Experimental results

The hydraulic jump flow was a sudden transition from rapid to fluvial flow motion characterised by the development of large-scale turbulence, surface waves and air entrainment. Air bubbles were entrained at the jump toe into a free shear layer characterised by intensive turbulence production (Figs. 1, 2). The entrained air packets were broken up in very small air bubbles as they were advected in the developing shear region. Once the bubbles were convected into regions of lesser shear, bubble collisions and coalescence led to larger air entities (bubbles, pockets) that were driven by buoyancy upwards to the free surface. In the recirculation region above the mixing layer, strong unsteady flow reversals occurred.

Vertical profiles of void fraction C and bubble count rate F were measured at different longitudinal positions $4.1 < (x-x_1)/d_1 < 34$. Figures 3 and 4 present some typical results, where the present data are compared with the earlier data of Chanson (2006). In the developing shear layer, the data compared favourably with an analytical



Fig. 2 Bubble entrainment in hydraulic jumps. **a** $Fr_1 = 5$, $Re = 38,000$, $x_1 = 0.75$ m, $d_1 = 0.018$ m, shutter speed: 1/40 s, flow from right to left. **b** $Fr_1 = 8.3$, $Re = 62,000$, $x_1 = 0.75$ m, $d_1 = 0.018$ m, shutter speed: 1/80 s, flow from right to left. The phase-detection probe is visible above the recirculation region

solution of the advective diffusion equation for air bubbles (Chanson 1997):

$$C = C_{\max} \exp \left(- \frac{((y - y_{C_{\max}})/d_1)^2}{4D^*(x - x_1)/d_1} \right) \quad (5)$$

where C_{\max} is the maximum void fraction in the shear layer, $y_{C_{\max}}$ is the vertical elevation of the maximum void fraction C_{\max} , D^* is a dimensionless turbulent diffusivity: $D^* = D_t/(V_1 d_1)$, D_t is the air bubble turbulent diffusivity. Equation (5) is compared with some data in Figs. 3a, 4a and c. The peak of void fraction C_{\max} was clearly marked for most investigated conditions (Table 1), but at the lowest Reynolds numbers for $Fr_1 = 5.1$.

Figures 3b, 4b and d present some typical vertical distributions of dimensionless bubble count rate $F d_1/V_1$. The bubble count rate F is defined the number of air bubbles detected by the probe-leading sensor per unit time and it is proportional to the specific air–water interface area. All the data exhibited a major peak of bubble count rate F_{\max} in the developing shear region. It is suggested that this peak was linked with high levels of turbulent shear stresses that break up the entrained air bubbles into finer air entities. Figure 4 shows further some results at two dimensionless longitudinal positions. A comparison between Fig. 4a and c, and between Fig. 4b and d, illustrates the de-aeration of the flow with increasing distance from the jump toe.

Figure 5 shows some dimensionless bubble chord time probability distribution functions in the developing shear layer. The data were recorded at the location where the bubble count rate was maximum ($F = F_{\max}$). For each figure, the caption provides the location $((x-x_1)/d_1, y/d_1)$, local air–water flow properties (C, F), and number of recorded bubbles N_{ab} . The bubble chord time was proportional to the bubble chord length and inversely proportional to the velocity. Small bubble chord times corresponded to small bubbles passing rapidly in front the probe sensor, while large chord times implied large air packet flowing slowly past the probe sensor. For intermediate chord times, there were a wide range of possibilities in terms of bubble sizes depending upon the bubble velocity. The present results showed a number of typical trends: (a) a broad spectrum of bubble chord time at each location, (b) a preponderance of small bubble chord times relative to the mean with a shape that followed in average a log–normal distribution, and (c) a similar shape at most vertical elevation y/d_1 in both shear and recirculation regions.

4 Dynamic similarity in air–water flow properties

The present experiments were compared with the earlier data sets of Chanson (2006). The three data sets were

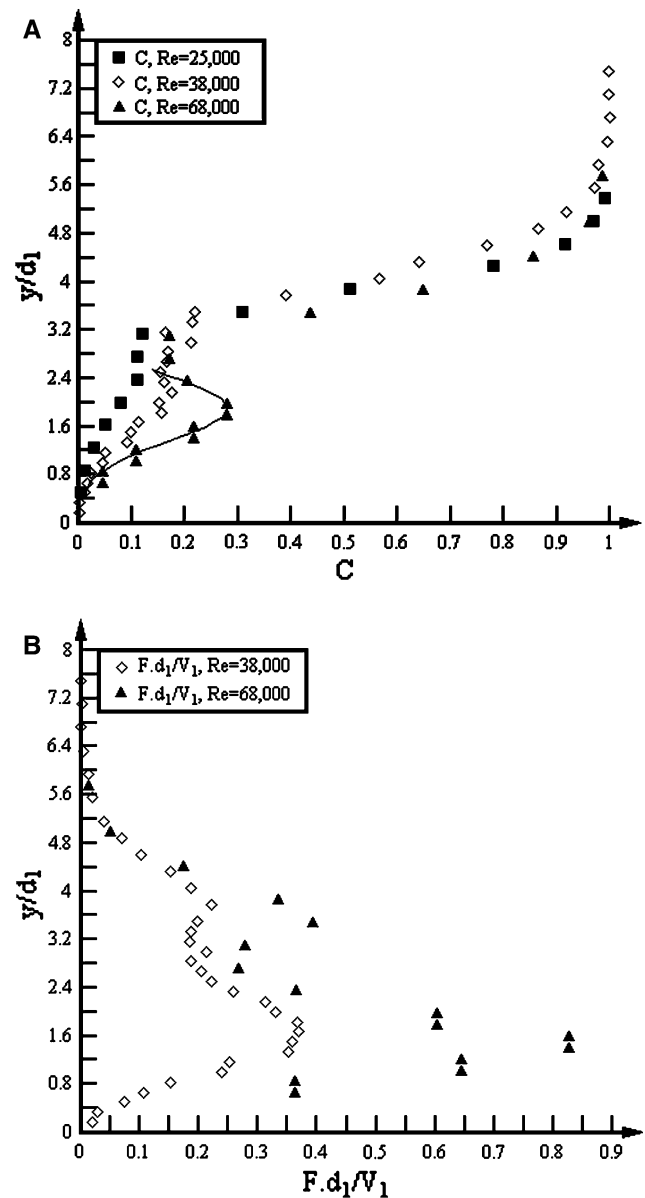


Fig. 3 Dimensionless distributions of void fraction and bubble count rate in the hydraulic jump for $Fr_1 = 5.1$, $x_1/d_1 = 42$, $W/d_1 \geq 20$ and $(x-x_1)/d_1 = 8$, $Re = 25,000, 38,000$ and $68,000$ —data: Chanson (2006) and present study ($Re = 38,000$). **a** Void fraction data—comparison with Eq. (5) (solid line). **b** Dimensionless bubble count rate data $F d_1/V_1$

designed to be geometrically similar based upon a Froude similitude with undistorted scale (Table 1). The geometric scaling ratio was $L_{\text{scale}} = 2.0$ between the largest and smallest series of experiments ($d_1 = 0.024$ and 0.012 m, respectively), where L_{scale} is the geometric scaling ratio defined as the ratio of prototype to model dimensions, and $L_{\text{scale}} = 1.33$ between the largest series of experiments and the present data set ($d_1 = 0.024$ and 0.018 m, respectively). Similar experiments were conducted for two inflow Froude numbers $Fr_1 = 5$ and 8.5 with identical upstream

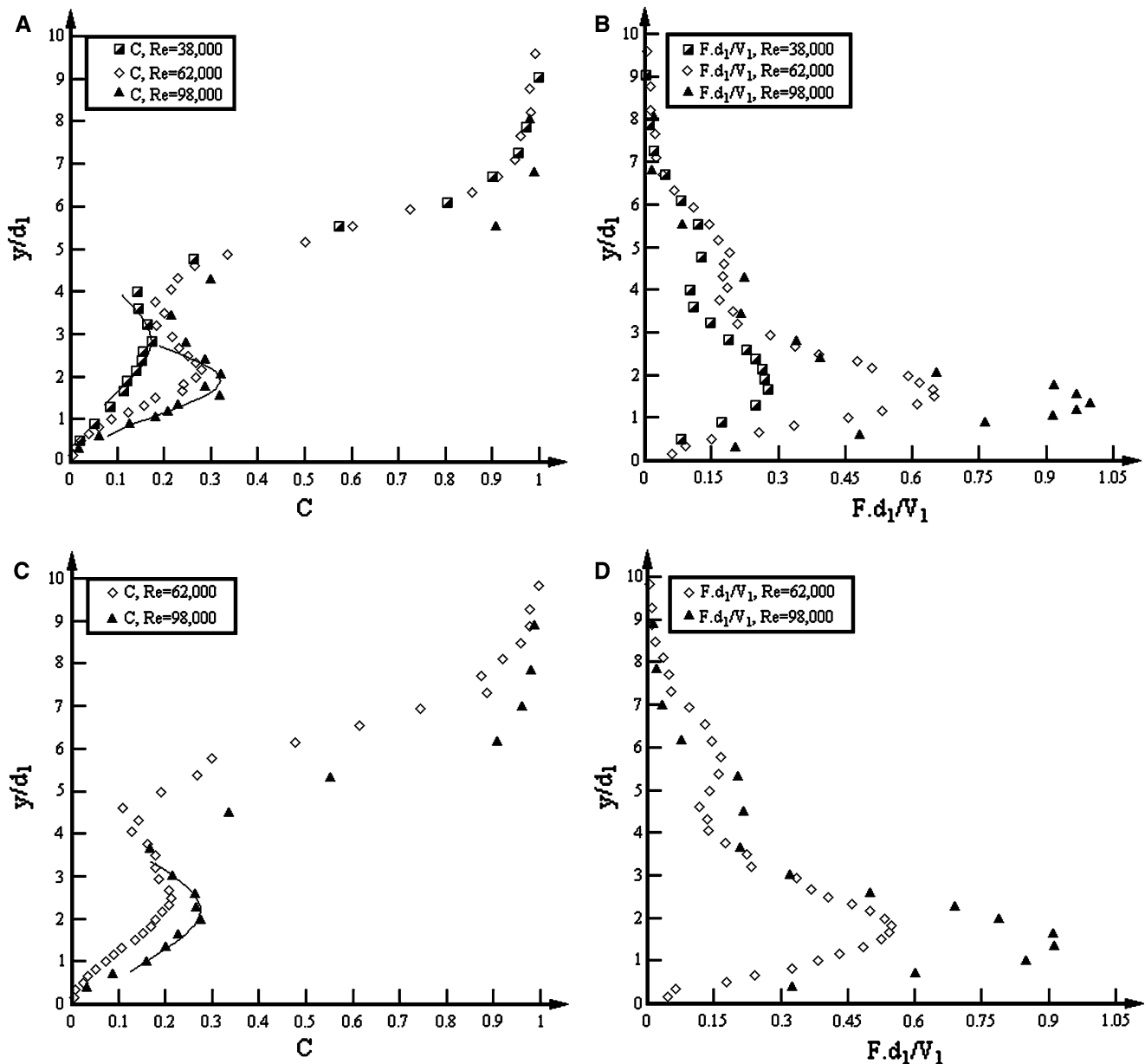


Fig. 4 Dimensionless distributions of void fraction and bubble count rate in the hydraulic jump for $Fr_1 = 8.5$, $x_1/d_1 = 42$, $W/d_1 \geq 20$ and $Re = 38,000$, $62,000$ and $98,000$ —data: Chanson (2006) and present study ($Re = 62,000$). **a** $(x-x_1)/d_1 = 12$, void fraction data—

comparison with Eq. (5) (solid line). **b** $(x-x_1)/d_1 = 12$, bubble count rate data $F \cdot d_1 / V_1$. **c** $(x-x_1)/d_1 = 17$, void fraction data—comparison with Eq. (5) (solid line). **d** $(x-x_1)/d_1 = 17$, bubble count rate data $F \cdot d_1 / V_1$

distance x_1/d_1 between gate and jump toe, and with Reynolds numbers ranging from 25,000 to 98,000. For a given Froude number, the two-phase flow measurements were performed in the developing air–water flow region at identical cross-sections $(x-x_1)/d_1 \leq 34$.

Typical comparative results are presented in Figs. 3, 4 and 5. The data showed drastic scale effects in the smaller hydraulic jumps in terms of void fraction and bubble count rate distributions. The results highlighted consistently a more rapid de-aeration of the jump roller with decreasing

Reynolds number for a given inflow Froude number, an absence of self-similarity of the void fraction profiles in the developing shear layer for $Re < 40,000$ and $Fr_1 = 5$ (Fig. 3a), and an increasing dimensionless bubble count rate with increasing Reynolds number for a given inflow Froude number (Figs. 3b, 4b). In Fig. 3a, the distributions of void fraction in the shear layer followed Eq. (5) for $Re = 68,000$ but were basically flat for $Re = 25,000$ and $38,000$. The bubble chord time distributions were not scaled according to a Froude similitude. Comparatively

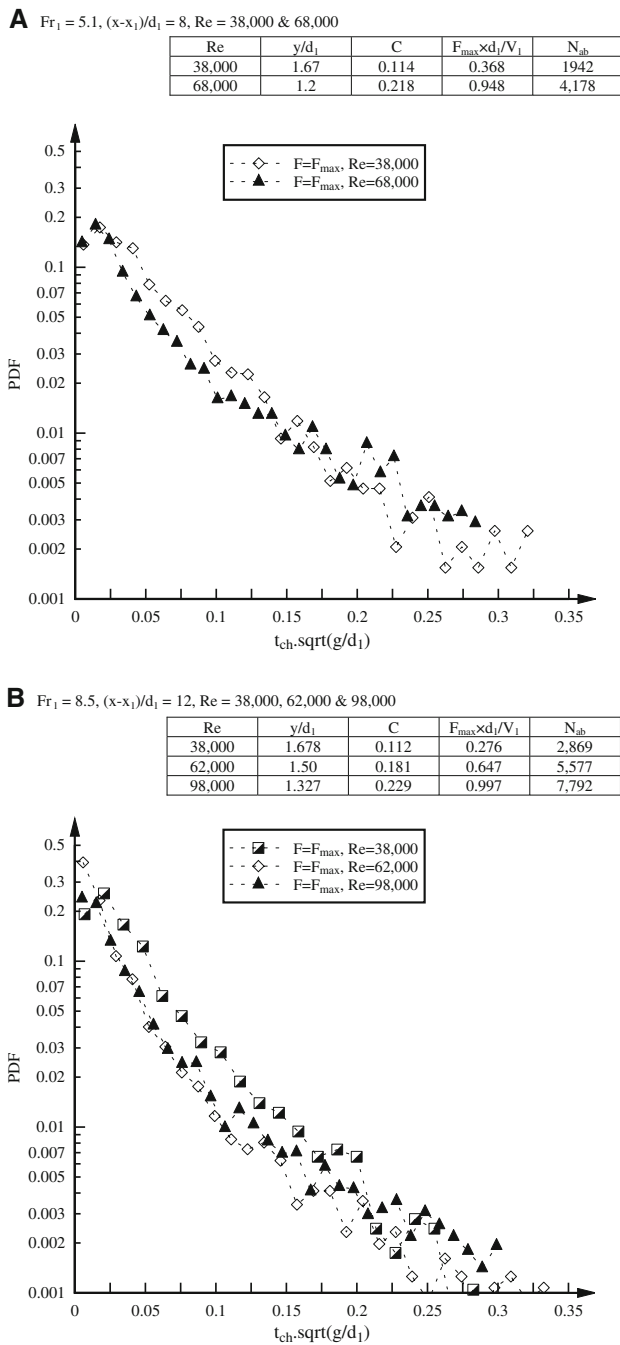


Fig. 5 Dimensionless probability distribution functions of bubble chord time $t_{ch} \sqrt{g/d_1}$ in the developing shear layer of hydraulic jumps at $F = F_{max}$ for $x_1/d_1 = 42, W/d_1 \geq 20$ and $Re = 38,000, 62,000, 98,000$ —data: Chanson (2006) and present study ($Re = 62,000$)

larger bubble chord times were observed at low Reynolds numbers (Fig. 5a, b).

The effects of the Reynolds number on the two-phase flow properties were particularly marked in the developed shear layer. This is illustrated in Fig. 6 showing the maximum void fraction C_{max} and maximum dimensionless bubble count rate $F_{max} d_1/V_1$ in the shear layer as functions

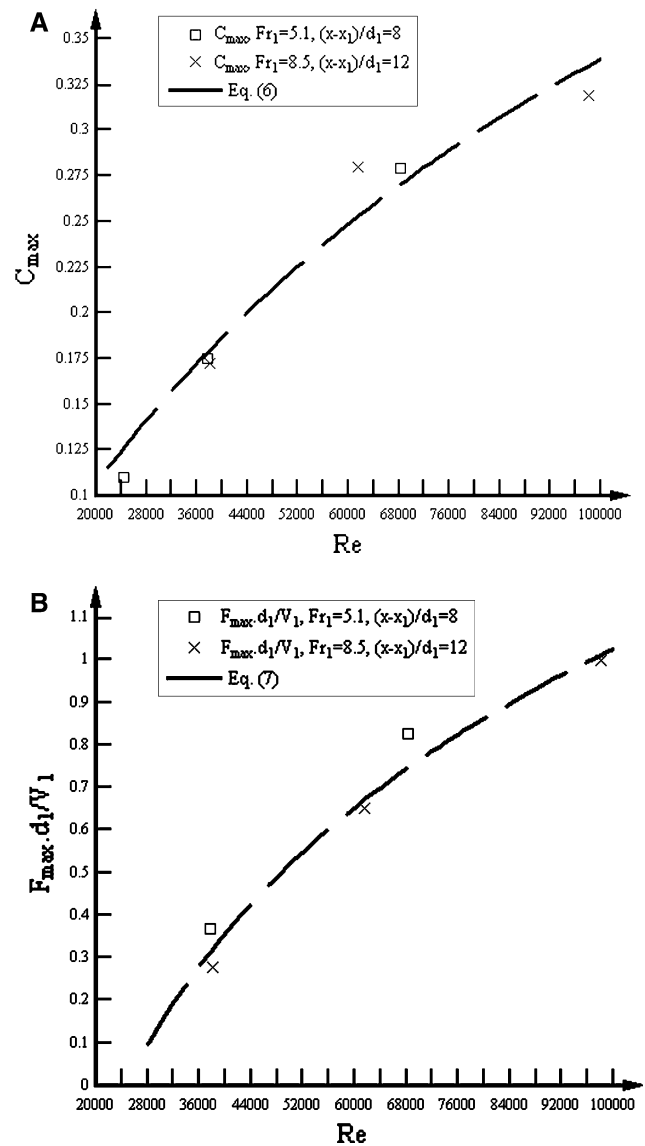


Fig. 6 Effects of the inflow Reynolds number on the maximum void fraction C_{max} and maximum dimensionless bubble count rate $F_{max} d_1/V_1$ in the developing shear layer—data: Chanson (2006) and present study. **a** Maximum void fraction C_{max} —comparison with Eq. (6). **b** Maximum bubble count rate $F_{max} d_1/V_1$ —comparison with Eq. (7)

of the inflow Reynolds number Re . Figure 6a presents the relationship between C_{max} and Re , and Fig. 6b shows the variation of $F_{max} d_1/V_1$ with Re . The results highlighted some monotonic increase in maximum void fraction and maximum dimensionless bubble count rate in the mixing layer with increasing Reynolds number. The rate of increase was about the same for both inflow Froude numbers $Fr = 5$ and 8.5 . Further no asymptotic limit was observed within the range of the experiments (Table 1). The relationships in maximum void fraction and bubble count, and Reynolds number were correlated by:

$$C_{\max} = \frac{0.745Re}{Re + 1.20 \times 10^5} \quad 2 \times 10^4 < Re < 10^5 \quad (6)$$

$$\frac{F_{\max} d_1}{V_1} = 0.73 \times \ln(Re) - 7.38 \quad 2 \times 10^4 < Re < 10^5 \quad (7)$$

with a normalised coefficient of correlation of 0.978 and 0.984, respectively.

The comparative analysis highlighted that (1) the experimental data obtained with $Re = 25,000$ could not be scaled up to $Re = 98,000$, and that (2) the data sets with Reynolds numbers up to 98,000 could not be extrapolated to large-size prototype structures without significant scale effects in terms of void fraction and bubble count rate distributions. This result has important implications in terms of civil, environmental and sanitary engineering design. In hydraulic structures, storm water systems and water treatment facilities, hydraulics jumps operate typically with inflow Reynolds numbers ranging from 10^6 to over 10^8 .

5 Conclusion

Detailed air–water flow measurements were conducted in hydraulic jumps with partially developed inflow conditions. The void fraction distributions showed the presence of an advective shear layer in which the air concentration distributions followed an analytical solution of the diffusion equation, while the bubble count rate distributions exhibited a marked maximum in the mixing layer. Similar experiments were conducted with identical inflow Froude numbers ($Fr_1 = 5$ and 8.5) and Reynolds numbers between 24,000 and 98,000 (Table 1). The results of Froude-similar experiments showed some drastic scale effects in the smaller hydraulic jumps in terms of void fraction, bubble count rate and bubble chord time distributions. Void fraction distributions implied comparatively greater detrainment at low Reynolds numbers yielding to lesser overall aeration of the jump roller, while an absence of self-similarity was observed for $Fr_1 = 5$ and $Re < 40,000$. The dimensionless bubble count rates were significantly lower at low Reynolds numbers, especially in the mixing layer. The bubble chord times were comparatively larger at low Reynolds numbers.

In a physical model, the flow conditions are said to be similar to those in the prototype if the model displays similarity of form, similarity of motion and similarity of forces. Equation (1) highlighted that the study of air bubble entrainment in hydraulic jumps required a large number of relevant parameters. The present comparative analysis demonstrated quantitatively that dynamic similarity of two-phase flows in hydraulic jumps cannot be achieved with a Froude similitude unless working at full-scale (1:1). In experimental facilities with Reynolds numbers up to 10^5 ,

some viscous scale effects were observed in terms of the rate of entrained air, air–water interfacial area and bubble size populations.

Acknowledgments The writers acknowledge the technical assistance of Graham Illidge and Clive Booth. The first writer acknowledges the financial support of the ESTACA and particularly François Stephan (Head of Department).

References

- Bélanger JB (1828) Essai sur la Solution Numérique de quelques Problèmes Relatifs au Mouvement Permanent des Eaux Courantes. *Carilian-Goëury*, Paris, France (in French)
- Chanson H (1995) Air entrainment in two-dimensional turbulent shear flows with partially developed inflow conditions. *Int J Multiphase Flow* 21(6):1107–1121
- Chanson H (1997) Air bubble entrainment in free-surface turbulent shear flows. Academic Press, London, 401 p
- Chanson H (2002) Air–water flow measurements with intrusive phase-detection probes. Can we improve their interpretation?. *J Hydraulic Eng Trans ASCE* 128(3):252–255
- Chanson H (2006) Air bubble entrainment in hydraulic jumps. Similitude and scale effects. Report No. CH57/05, Department of Civil Engineering, The University of Queensland, Brisbane, 119 p
- Chanson H (2007a) Bubbly flow structure in hydraulic jump. *Euro J Mech B/Fluids* 26(3):367–384
- Chanson H (2007b) Dynamic similarity and scale effects affecting air bubble entrainment in hydraulic jumps. In: Sommerfield M (ed) Proceedings 6th international conference on multiphase flow ICMF 2007, Leipzig, Germany, July 9–13, Session 7, Paper S7_Mon_B_S7_Mon_B_3, 11 pages (CD-ROM)
- Chanson H, Brattberg T (2000) Experimental study of the air–water shear flow in a hydraulic jump. *Int J Multiphase Flow* 26(4):583–607
- Chanson H, Carosi G (2007a) Turbulent time and length scale measurements in high-velocity open channel flows. *Exp Fluids* 42(3):385–401. doi:10.1007/s00348-006-0246-2
- Chanson H, Carosi G (2007b) Advanced post-processing and correlation analyses in high-velocity air–water flows. *Environ Fluid Mech* 7(6):495–508. doi:10.1007/s10652-007-9038-3
- Chanson H, Gualtieri C (2008) Similitude and scale effects of air entrainment in hydraulic jumps. *J Hyd Res IAHR* 46(1):35–44
- Crowe C, Sommerfield M, Tsuji Y (1998) Multiphase flows with droplets and particles. CRC Press, Boca Raton, 471 p
- Henderson FM (1966) Open channel flow. MacMillan Company, New York
- Mossa M, Tolve U (1998) Flow visualization in bubbly two phase hydraulic jumps. *J Fluids Eng Trans ASME* 120:160–165
- Murzyn F, Chanson H (2007) Free surface, bubbly flow and turbulence measurements in hydraulic jumps. Report No. CH63/07, Division of Civil Engineering, The University of Queensland, Brisbane, July, 116 p
- Murzyn F, Mouazé D, Chaplin JR (2005) Optical fibre probe measurements of bubbly flow in hydraulic jumps. *Int J Multiphase Flow* 31(1):141–154
- Murzyn F, Mouazé D, Chaplin JR (2007) Air–water interface dynamic and free surface features in hydraulic jumps. *J Hydraulic Res IAHR* 45(5):679–685
- Rajaratnam N (1962) An experimental study of air entrainment characteristics of the hydraulic jump. *J Inst Eng India* 42(7): 247–273

- Resch FJ, Leutheusser HJ (1972) Le Ressaut Hydraulique: mesure de Turbulence dans la Région Diphasique. *La Houille Blanche* No. 4, pp 279–293 (in French)
- Toombes L (2002) Experimental study of air–water flow properties on low-gradient stepped cascades. In: PhD thesis, Department of Civil Engineering, The University of Queensland, Brisbane
- Wood IR (1991) Air entrainment in free-surface flows. IAHR hydraulic structures design manual no. 4, hydraulic design considerations, Balkema Publ., Rotterdam, 149 p